IDŐJÁRÁS

Quarterly Journal of the Hungarian Meteorological Service
Vol. 105, No. 4 — Vol. 106, No. 1, October 2001 — March 2002, pp. 243-251

High accuracy skin temperature retrieval from spectral data of multichannel IR imagers

Ferenc Miskolczi

Science Applications International Corporation,
1 Enterprise Pkwy, Suite 300, Hampton, VA 23666, USA
E-mail: f.m.miskolczi@larc.nasa.gov

(Manuscript received November 14, 2001)

Abstract—The increasing number of IR spectral channels of recent satellite imagers implies the more accurate retrieval of surface skin temperature. In this paper the theoretical accuracy limits as a function of channel numbers, viewing angles and noise equivalent radiances have been studied. Based on LBL computations of the channel radiances regression type relationships have been established between the brightness temperatures and the skin-temperatures. In this study model filter functions of the 7 IR channels of the GLI imager of the ADEOS-I have been used with a large set of temperature profiles. The global and seasonal distribution of temperature profiles were considered by groups of climatologically representative temperature profiles. Standard singular value decomposition program package was used to solve the multivariable linear regression problem. Results show that the accuracy limits of the skin temperature retrievals are depending mainly on the noise equivalent radiances and up to around 60 degree viewing angles remaining in the range of 0.1–0.2 K.

Key-words: remote sensing, skin temperature, ADEOS

1. Introduction

Satellite based remote sensing of the Earth-atmosphere system has an increasing role in climate change detection. Imager instruments have nowadays improved accuracy and more channels allowing the development of better retrieval algorithms for a variety of surface and atmospheric parameters. The first step in the retrieval of the surface temperature is to derive the accurate skin temperature from the radiance measurements. Formerly, with imagers using one or two spectral channels, accuracy was limited. The necessary information on the characteristics and involvement of the H_2O and other molecular species in the windows absorption was unavailable. The Global Imager, (GLI), on board the Advanced

Earth Observing Satellite, (ADEOS 2), offers four window channels and three H_2O channels for better surface temperature detection with a possibility of obtaining information on the initial trend of the moisture profile. In the present paper, the theoretical accuracy limits of the clear-sky skin temperature retrievals using the GLI infrared channels have been established, based on high resolution radiative transfer computations and regression analysis.

2. Method

For a given filter function the average wave number, the effective wave number and the channel radiance are expressed as:

$$\nu_k^a = \frac{\int_{\Delta\nu} \nu \Phi_k(\nu)\, d\nu}{\int_{\Delta\nu} \Phi_k(\nu)\, d\nu}, \tag{1}$$

$$\nu_k^e = \frac{\int_{\Delta\nu} \nu I(\nu)\, \Phi_k(\nu) d\nu}{\int_{\Delta\nu} I(\nu)\, \Phi_k(\nu)\, d\nu}, \tag{2}$$

and

$$I_k = \frac{\int_{\Delta\nu} I(\nu) \Phi_k(\nu) d\nu}{\int_{\Delta\nu} \Phi_k(\nu) d\nu}, \tag{3}$$

where $I(\nu)$ is the spectral radiance, $\Phi_k(\nu)$ is the filter function, ν is the wave number and the subscript k refers to the serial number of the spectral channel. In *Table 1* the GLI and GOES-8 filter functions are compared. Some GOES-8 channels are close to the corresponding GLI channels, therefore the results and conclusions could also be valid for those filters.

Table 1. Average wave numbers, ν_k^a, and half widths, β_k, of the GLI engineering model filter functions and some similar GOES-8 filter functions (units are in cm^{-1})

	GLI		GOES-8	
No.	ν_k^a	β_k	ν_k^a	β_k
1	836.47	52.52	835.97	64.18
2	945.83	69.60	934.75	86.06
3	1160.30	72.12		
4	1377.06	94.67		
5	1430.78	97.10		
6	1484.88	113.60	1482.04	122.76
7	2699.92	239.34	2559.44	165.62

Skin temperature retrieval using regression type relationships between the channel scene temperatures and the true radiative temperatures of the surface is very simple:

$$T = \alpha_0 + \sum_{k=1}^{N} \alpha_k T_k^c , \tag{4}$$

where T is the skin temperature, N is the number of the spectral channels, α_k's are regression coefficients and T_k^c's are the estimated scene temperatures. T_k^c's are computed from the brightness temperatures and they are supposed to be corrected for the shift in the effective wave number with the change in the structure of the spectral radiance. The brightness temperatures are computed from the channel radiances via the inverse Planck function and using the average wave number. The "accurate" scene temperature is computed the same way, but using the effective wave number. In case of an ideal black body radiance spectra, the magnitudes of the brightness temperature corrections at different GLI channels are presented in *Fig. 1*.

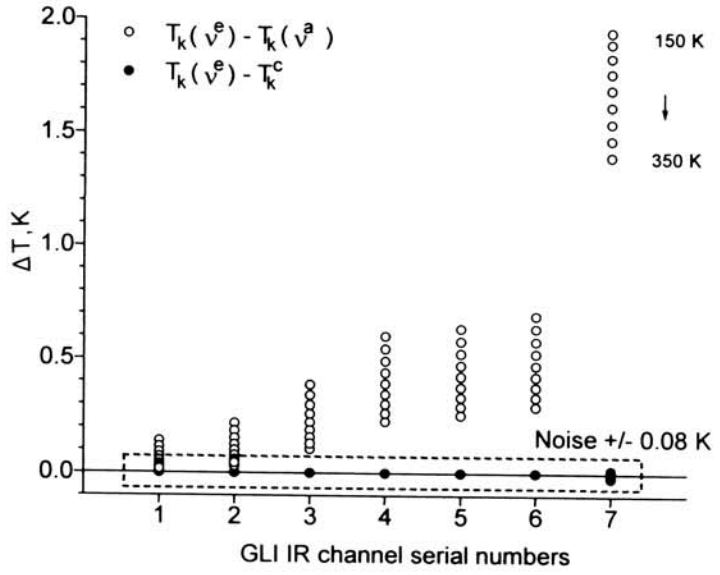

Fig. 1. Brightness temperature corrections using ideal black body functions in the range of 150–350 K. The dashed line is an assumed average noise level of the IR channels.

To perform the corrections there are several methods. NOAA uses linear (or more recently second order polynomial) fit, *Weinreb et al.* (1997). For the GLI channels we applied a logarithmical fit to express the effective wave number as the function of the channel radiance:

$$T_k^c = B^{-1}(v_k^c, I_k), \tag{5}$$

where

$$v_k^c = c_k^1 + c_k^2 \ln(I_k). \tag{6}$$

In the above equations v_k^c is the estimated effective wave number, c_k^1 and c_k^2 are regression coefficients. Eq. (5) and (6) proved to be more accurate, (not shown here), and uses less coefficients than the NOAA method. Brightness temperature corrections based on ideal black body radiation is not justified when the distribution of the spectral radiance does not follow the Planck's radiation law. In the present work the c_k^1 and c_k^2 regression coefficients were determined using real atmospheric radiance spectra. Obviously, since the degree of modulation of the ideal black body spectra is dependent on the optical path within the atmosphere, for correct scene temperature computations a set of regression coefficients are needed for different viewing angles.

In *Fig. 2*, the brightness temperature corrections as the function of the channel radiances are plotted for the GLI channel 6. The correction error is the difference between the corrections, $(T_k - T_k^c)$, using ideal black body type or real atmospheric spectra in Eqs. (5) and (6). In this channel, Fig. 2 shows a large (–0.68 K) bias, and actually suggests not to use any corrections based on ideal black body radiance spectra. The situation in the GLI channel 7 is similar, but with a bias of 0.5 K. In channel 1 and 2 the biases remain below the noise level.

In general, the success of the regression scheme given in Eq. (4) is entirely dependent on the accuracy of the computed channel radiances and the statistical representativeness of the atmospheric temperature, water vapor, ozone and other trace gas profiles.

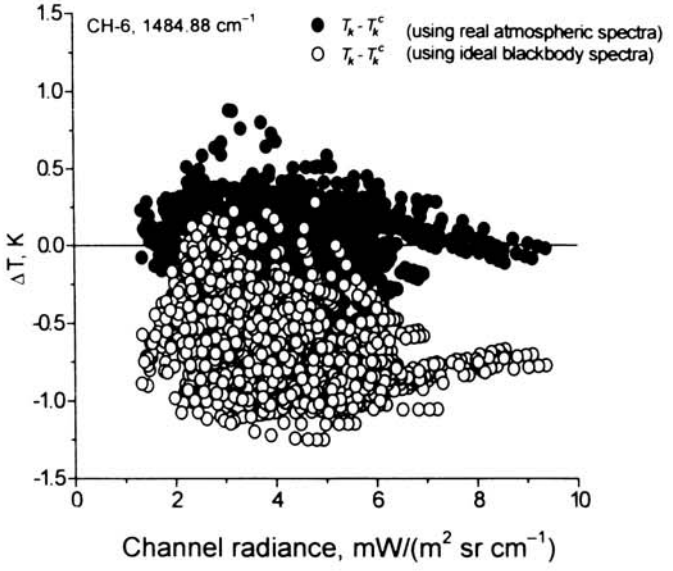

Fig. 2. Scene temperature error in the GLI water vapor channel due to the different brightness temperature correction methods.

3. *Regression data set*

The present study uses a subset of the TOVS Initial Guess Retrieval (TIGR), database of 1761 radiosonde observations (*Chedin* and *Scott*, 1983). This data set contains the pressure, temperature, H_2O and O_3 mixing ratio profiles at 40 pressure levels between 0.05 and 1013 hPa. The soundings were collected over both hemispheres and over all seasons from 1976. In *Table 2* the characteristics of the original data set are summarized.

Table 2. Average characteristics of the TIGR subset containing 1761 profiles in 11 classes (M is the number of profiles, u is in prcm, T_e is in K and p_e is in hPa)

	Region and season	M	u	T_e	P_e
1	Arctic summer	112	1.0	263	795
2	Arctic winter	295	0.3	250	779
3	North midlatitude summer	57	2.7	281	797
4	North midlatitude fall/spring	88	1.1	266	804
5	North midlatitude winter	332	0.9	263	804
6	North/South tropical	114	3.6	285	816
7	South midlatitude summer	131	1.6	271	808
8	South midlatitude fall/spring	155	1.0	264	805
9	South midlatitude winter	151	1.1	269	823
10	Antarctic summer	157	0.5	255	783
11	Antarctic winter	169	0.3	250	774

To obtain the best retrieval on a global scale, the profiles were classified according to their geographical latitudes and the seasons. Based on the latitudinal and annual distribution, 5 latitudinal belts were selected, and in each belt, one, two or three "seasons" were established, roughly based on the solar climate. Because of the apparent asymmetry in the global and seasonal distribution of the available solar radiation, the northern and southern hemispheres were treated separately. This classification of profiles resulted in 11 groups with a minimum of 57 profiles during the northern midlatitude summer, and a maximum of 331 profiles during the northern midlatitude winter. Further on, for practical reasons, it was necessary to reduce the number of the profiles to a reasonably small number, suitable for detailed line-by-line calculations. Due to the fact that the window channel radiances are affected mainly by the absorption of atmospheric water vapor, the selection of the individual TIGR profiles was based on the total precipitable water, u, effective H_2O temperature, T_e, and effective H_2O pressure, p_e. The effective values were computed by weighting the temperature and pressure profiles with the water vapor column density profile. A pre-selection based on the

statistical characteristics of the 11 groups resulted in 297 profiles. The extreme profiles from each group (profiles closest to the average +/- three standard deviations) have been excluded on the basis that we did not want the regression coefficients to be affected by some statistically insignificant rare cases. After eliminating the redundancies the final set has been reduced to 228 profiles. This set contained approximately 20 profiles in each class and has a similar statistical pattern to the original dataset.

4. Radiative transfer computation

For the radiance computations the High Resolution Radiative Transfer Code (HARTCODE) was used with the GEISA 97 absorption line catalog (*Miskolczi et al.*, 1990). In addition to the H_2O and O_3, there are nine molecular species that exhibit significant absorption in the GLI IR channels. The volume mixing ratio profiles of these absorbers (CO_2, N_2O, CH_4, NO, SO_2, NO_2, CCl_4, F11 and F12) were taken partly from the seasonal standard atmospheres. CCL_4, F11 and F12 mixing ratio profiles were measured at the Oklahoma ARM site. To create a physically consistent data set, after merging the additional absorbers into the TIGR profiles, a new exponential layering was introduced. The top altitude was set to 61.2 km and the number of the layers were reduced to 32. The new layers have a geometrical thickness of about 100 m at the bottom and 10 km at the top. The outgoing radiances were computed with 1 cm^{-1} spectral resolution in 9 different viewing angles, which makes a total of 2052 high resolution radiance spectra. In the convolution of the radiance spectra with the filter functions, the radiance spectra were interpolated to the higher resolution discrete points of the filter functions. The 1 cm^{-1} resolution was sufficient for the accurate evaluation of channel radiances in Eq. (3). The α_k regression coefficients in Eq. (4) were determined by singular value decomposition. In the present study, the first 6 GLI channels were utilized and in each group of profiles 9 set of regression coefficients were generated for each viewing angle. The reason of using 9 set of coefficients for 9 different viewing angles is in the fact that no uniform limb darkening function exists, even within one group of profiles. The best retrieval results are expected by using interpolated regression coefficients with respect to the viewing angles.

5. Results

According to test computations, the derived α_k regression coefficients were very stable, they were not sensitive to a 0.2 K white noise added to the scene temperatures, therefore, the regression coefficients were assumed to be error free. There

is no effect of the brightness temperature correction on the accuracy of the retrieval. This is expected, since the standard error in a linear regression scheme is invariant for the linear transformations of the variables. However, the use of brightness temperature instead of channel radiance improves the explained variance by about 4 to 5 per cent. It is interesting to note that the conversion of channel radiances into brightness temperatures or scene temperatures is not always beneficial. For example, in retrieving water vapor effective pressure, p_e, it is better to use directly the channel radiance. In *Figs. 3, 4* and *5* the different kinds of errors of the skin temperature retrievals as the function of the viewing angles are displayed. In all cases the computations were based on the estimated scene temperatures using Eqs. (5).

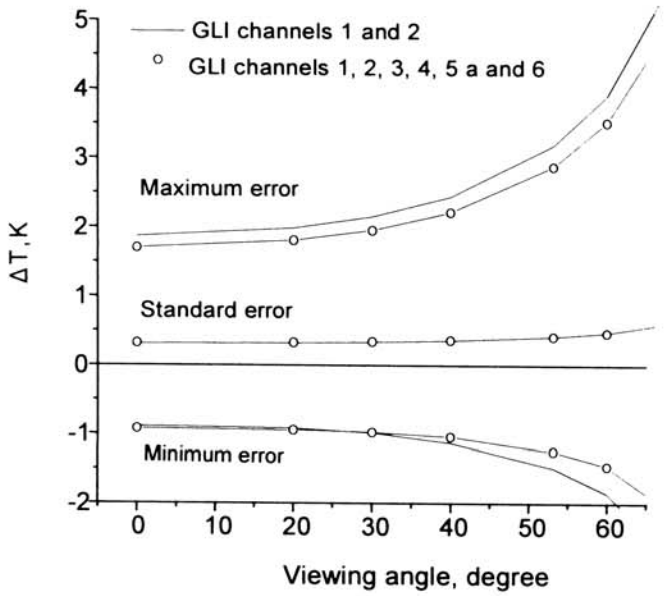

Fig. 3. Skin temperature errors in case of applying two or six spectral channels in the retrievals. (Full data set, no classes, 0.1 K noise.)

Fig. 3. shows the dependence of the errors on the number of the channels involved in the retrieval. In this case all the profiles in the 11 classes were merged into one large group of 228 profiles. It is surprising that adding an additional window channel and the three water vapor channels has no noticeable effect on the standard error, however, the minimum and maximum errors were slightly reduced. Probably there is a better way to use the information content of the excess channels than to include them directly into the regression scheme.

In Fig. 4 the effect of the grouping of the profiles are presented. Here the retrievals were based on the first 6 channels of the GLI. Apparently the accurate limb darkening corrections by using sets of regression coefficients for the different viewing angles are necessary to achieve an accuracy of around 0.1 K.

Fig. 5 shows the dependence of the errors on the noise equivalent temperatures. In this cases regression coefficients were generated for each class and viewing angle. The scene temperatures were loaded with a zero-mean white noise of different standard deviations. The close to linear degrading effect due to the measurement noise is obvious. The zero-noise curve at around 0.05 K can be regarded as a "theoretical" upper accuracy limit that can be obtained using simple linear regression methods.

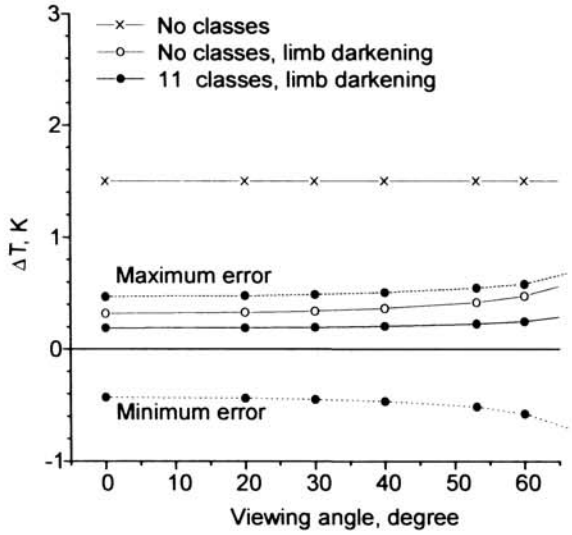

Fig. 4. Skin temperature errors in case of three different grouping. (2052 spectra in 1, 9 or 99 groups, 0.1 K noise.)

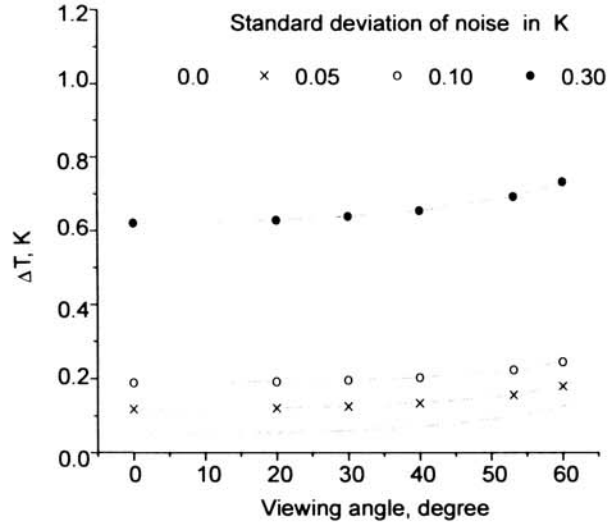

Fig. 5. Skin temperature errors in case of four different load of "white" noise.

6. Conclusions

Accurate skin temperature retrieval on global and annual scales can only be achieved by applying several sets of regression coefficients for the different regions, seasons and viewing angles. Limitations related to the instrument noise have been estimated. For the GLI instrument, assuming an average 0.08 K noise, the 0.3 K accuracy (in the sense of standard errors) is realistic. The target accuracy of the retrieval, using for example the GOES -10 imager, (assuming ~0.3 K noise and using less channels), could be around 0.6–0.8 K. Other conclusion is that sophisticated algorithms for the brightness temperature corrections using ideal black body, or even real atmospheric spectra, have no practical value when applying in a linear regression scheme. Further on, involving more H_2O and window channels into the retrieval will not increase the accuracy significantly. It seems that the only way of improvement is to reduce the noise in the spectral channels to or below 0.05 K.

References

Chedin, A. and *Scott, N., A.*, 1983: The improved initialization inversion procedure. *First International TOVS Study Conference*, Igls, Austria, August, 1983.

Miskolczi, F., Rizzi, R., Guzzi, R., and *Bonzagni, M*, 1990: High-resolution Radiance-Transmittance Code. *Meteor. Environ. Sci. Elsevier Pub. Co.* 743-790.

Weinreb, M.P., Jamieson, M., Fulton, N., Chen, Y., Johnson, J.X., Smith, B., and *Baucom, J.*, 1997: Operational calibration of geostationary operational environmental satellite imagers asounders. *Applied Optics 36*, 6895-6904.